International Journal of ISSI, Vol. 17(2020), No. 1, pp. 28-39

Oxidation Behavior of AISI 316 Steel Coated with Ni-P-TiO_2-Al_2O_3 Composite Coating

H. Ebrahimifar [1], F. Mohsenifar *[2]

[1]Department of Materials Engineering, Faculty of Mechanical and Materials Engineering, Graduate University of Advanced Technology, Kerman 7631133131, Iran
[2]Department of Mechanical Engineering, Higher Education Complex of Bam, Bam 7661314477, Iran

Abstract

Austenitic steels have numerous applications in high-temperature environments. The thermally-grown chromia scale on the steel surface may become unstable at high temperatures and as a result, oxidation resistance of steel will decrease. A potential method for improving oxidation properties is the use of composite coatings using techniques such as electroplating. In the present study, Ni-P-TiO_2-Al_2O_3 composite coating was deposited on AISI 316 steel substrate by electroplating. The as-coated samples were examined with scanning electron microscopy (SEM) with energy dispersive spectroscopy (EDS). X-ray diffraction (XRD) was also used to identify the formed phases in the as-coated structures. To evaluate oxidation behavior, isothermal oxidation, and cyclic oxidation were con-ducted at 800 ºC. Isothermal oxidation of uncoated steels revealed higher weight gain in comparison with Ni-P-TiO_2-Al_2O_3 composite-coated samples. The coating layer limited the outward diffusion of Cr cation and the inward diffusion of oxy-gen anion and resulted in a better oxidation resistance. According to the results of cyclic oxidation, coated substrates demonstrated excellent resistance against spallation and cracking.

Keywords: Composite coating, Electroplating, AISI 316 stainless steel, Oxidation.

1. Introduction

Among oxidation-resistant alloys, Fe-Cr-based alloys are preferred because of their low cost and high formability [1-3]. Stainless steels are used in various applications because of their acceptable performance in different environments. Stainless steels are employed in industry such as carbochemistry, petrochemical and power plants, gasification systems, combustion, aerospace, etc. [1-3]. During service at high temperatures, martensitic, ferritic, and austenitic steels can create a continuous chromium-oxide scale, which serves as a diffusion barrier against environmental attack. This surface layer is apt to destabilize above 1000 °C to the extent that it will not protect the substrate [4].

One of the best ways to improve corrosion and abrasion resistance is to apply surface coatings [4-7]. Among these coatings, nickel-base alloy and composite coatings are preferred [8-13].

Nickel coatings are widely used in the industry owing to their good adhesion to the substrate, thickness uniformity, and high hardness and wear resistance. But these coatings are brittle, and nickel on its own cannot provide good anti-corrosion and mechanical properties. To create better properties, composite coat-ings comprised of

**Corresponding author*
Email:F.mohseni@bam.ac.ir
Address:Department of Mechanical Engineering, Higher Education Complex of Bam, Bam 7661314477, Iran
1. Assistant Professor
2. M.Sc

nickel-base alloys are used [14-18]. This is achieved by the use of another element in the matrix and oxide particles as a second phase. In fact, by using secondary phases, the desired properties could be achieved, and by increasing or decreasing the percentage of secondary phases, the properties may arbitrarily change [4, 19].

Nowadays, nickel-phosphor coatings are being considered because of their high hardness, good corrosion resistance, and good oxidation resistance [7-11]. In previous studies, to improve oxidation resistance, abrasion resistance, and toughening, many scientists have investigated composite coatings containing nickel and secondary particles of TiO_2, Al_2O_3, SiC, CeO_2, and Fe_2O_3 [9,19,20].

Many studies have been carried out on Ni-Al_2O_3, Ni-Fe_2O_3, Ni-La_2O_3, and Ni-TiO_2 coatings [15, 21-27]. Abaei et al. [27] studied deposited Ni-Fe_2O_3 composite coatings on a 304 stainless steel substrate, and re-ported that this coating would improve the oxidation resistance of this steel. In another study, Khoran et al. [28] deposited Ni-TiO_2 composite coating on AISI 430 stainless steel by electroplating and reported that this composite coating was able to reduce the outward diffusion of chromium and improve the oxidation resistance of this steel.

Peng et al. [29, 30] investigated the oxidation behavior of Ni-La_2O_3 in comparison with pure nickel coatings. They reported that La_2O_3 prevented the removal of metal cations, and thus the coating had a better oxidation resistance than a pure nickel. Other researchers also investigated the oxidation behavior of Ni-Y_2O_3 in comparison with Ni-Al_2O_3 coating and reported that the former is better than the latter [32]. Vari-ous studies on the oxidation behavior of composite coatings have shown that oxidation behavior depends not only on the particle size but also on particle distribution [29-35].

In this study, Ni-P-TiO_2-Al_2O_3 composite coating was deposited on AISI 316 steel substrate using electro-plating. For investigating the oxidation behavior of 316 steel substrates and Ni-P-TiO_2-Al_2O_3 composite coating, isothermal oxidation tests were carried out on samples at 800 °C for 200 hours and cyclic oxidation at 800 °C for 50 cycles.

2. Experimental procedures

Samples with dimensions of 10 mm× 10 mm× 2 mm were cut from wrought AISI 316 stainless steel. The nominal chemical composition of AISI 316 stainless steel is listed in Table 1. Before coating, the sub-strates were polished from 400-grit SiC up to 1200-grit finish and then ultrasonically in acetone for 1 min. Chemical compositions and operating conditions for electrodeposition are given in Table 2. All chemicals were of analytic grade reagents (Merck). Contents of the electrolyte bath underwent sonication for about 15 min to break down agglomerates if present in the electrolyte bath. Then, the agglomeration of particles was prevented by a magnetic stirrer. The electrolyte temperature and pH value were set to 60°C and 3.5 respectively. For pH adjustment, either 0.1 mol/L sulfuric acid or sodium hydroxide was used. The cathode (steel substrate) and anode (nickel plate) were dipped into the electrolyte bath and kept 3 cm apart in a vertical position. The DC power supply was turned on and a current density of 15 mA/cm^2 was applied for 15 minutes. The electrolyte bath was kept agitated with a magnetic stirrer during electrodeposition. After electrodeposition, the applied current was turned off and the substrate was removed from the electrolyte bath. To remove the loosely bound extraneous materials from the coated surface, the sample was washed ultrasonically in distilled water for about 1 min. After cleaning with distilled water, the coated steel was dried in air and then weighed using an analytical balance. To evaluate the oxidation behavior; isothermal oxidation was carried out at 800°C. This test was performed in static air for up to 300 hours, specifically 12 uncoated and 12 Ni-P-TiO_2-Al_2O_3coated samples were pulled and weighted in dif-ferent exposure times, i.e., 5, 10, 20, 40, 60, 80, 100, 120, 150, 200, 250 and 300 hours. The uncoated and coated samples were also subjected to cyclic oxidation. Each cycle was composed of 1 h of heating in a furnace at 800 °C and 15 min of cooling in air. Microstructure and chemical composition of un-coated and Ni-P-TiO_2-Al_2O_3 coated specimens before and after oxidation were analyzed using scanning electron microscopy (SEM) (Oxford, model 7431) with energy dispersive spectroscopy (EDS). X-ray dif-fraction (XRD) was used to identify the formed phases in the surface layer of the as-coated and oxidized specimens with a Philips X'Pert High Score diffractometer using Cu Ka (λ= 1.5405 A). For all of the measurements,the samples were scanned in the 2θ range of 20–100°. The step angle and time step were kept at 0.02° and 1 sec/degree, respectively.

Table 1. Chemical composition of AISI 316 stainless steel (in wt. %).

Ni	Cr	Mo	Mn	C	Fe
10.9	16.6	002.04	1.85	0.07	balance

Table 2. Composition of coating mixtures and electrodeposition parameters/materials.

Coating mixtures		Electrodeposition parameters/materials	
$NiSO_4.6H_2O$	280.00 g/L	Current density	15 $mA.cm^{-2}$
$NiCl_2.6H_2O$	40.00 g/L	pH	3.5
H_3BO_3	40.00 g/L	Plating time	15 min
$NaPO_2H_2 \cdot H_2O$	15 g/L	Plating temperature	60 °C
SDS	0.3 g/L		
$C_7H_5NO_3S_1$	1 g/L		
Al_2O_3	1 g/L		
TiO_2	4 g/L		
		Cathode	AISI 316 stainless steel
		Anode	Nickel plate

3. Results and Discussion

3.1. Ni-P-TiO_2-Al_2O_3 Composite Coating

Fig. 1 shows the surface morphology SEM image of the Ni-P-TiO_2-$Al2O_3$ composite coating. The coat-ing is fully adherent on the substrate and there is no separation, discontinuity, and porosity on the coating. The presence of any cavity or porosity can reduce the adhesion of the coating to the substrate. In addition, the cavities allow corrosive components to pass through these paths and reach and react with the substrate. Also, no agglomeration is observed on the surface and the particles are uniformly distributed.

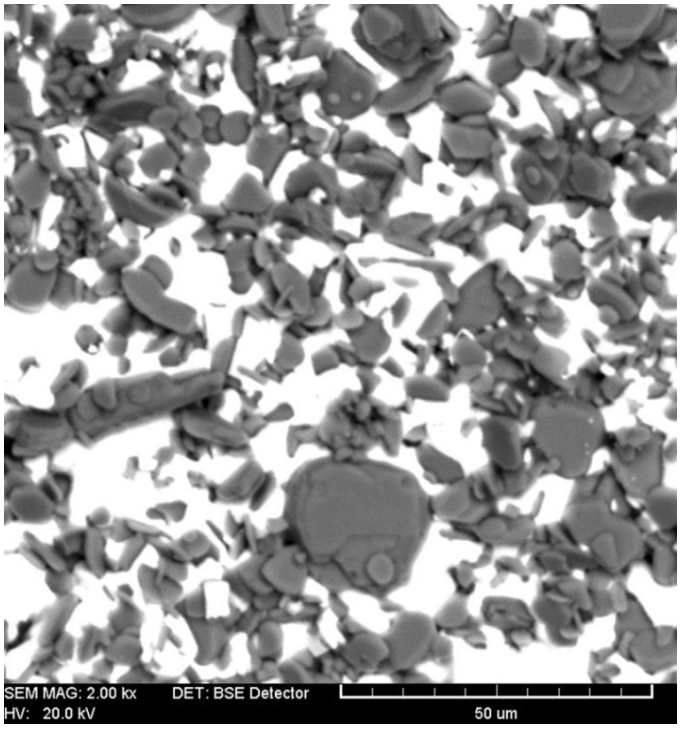

Fig. 1. SEM surface morphology of the Ni-P-TiO_2-Al_2O_3 composite coating.

Fig. 2 shows the distribution of the coating elements formed on the substrate. As can be seen, Ni, P, Ti, Al, and O are uniformly distributed. The uniform distribution of alloying elements shows no agglomeration. Fig. 3. shows the XRD analysis of the as-deposited Ni-P-TiO_2-Al_2O_3 composite coating. The phases which exist in the coating include Ni, Ni_5P_2, TiO_2, and Al_2O_3. Fig. 4 shows SEM cross section image (Fig. 4a) and concentration profiles of Ni, P, Ti, Al, O, Fe, and Cr (Fig. 4b) through the coating layer (Fig. 4b). As seen, there is a single uniform and distinct layer with the thickness of about 65 micrometers. There is no separation, discontinuity, and porosity between the substrate and Ni-P-TiO_2-Al_2O_3 composite coating.

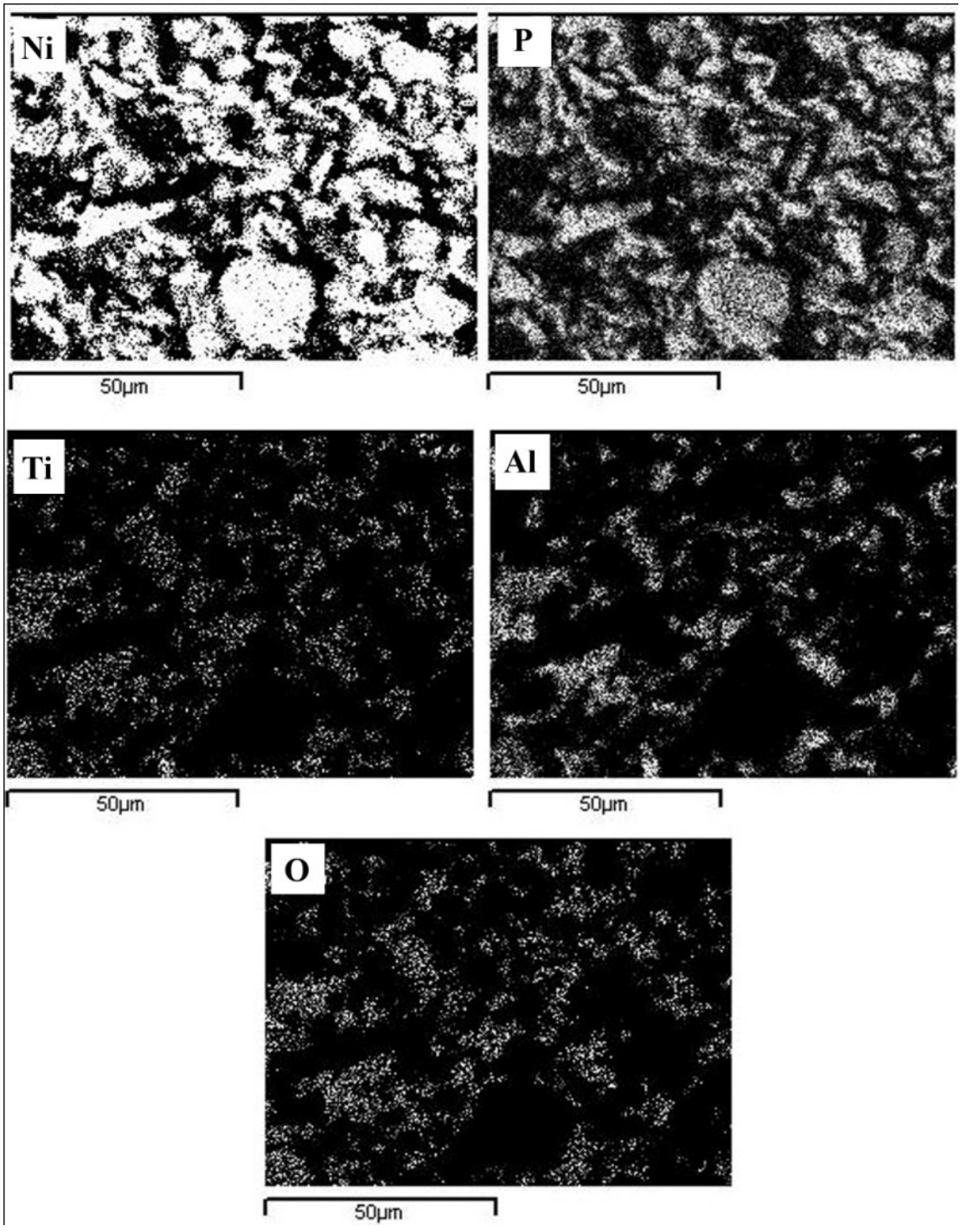

Fig. 2. Distribution of Ni, P, Ti, Al and O alloying elements inNi-P-TiO_2-Al_2O_3 composite coating.

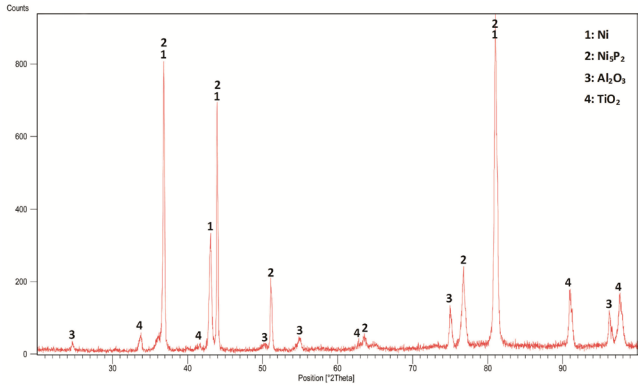

Fig. 3. XRD analysis of the sample coated with Ni-P-TiO_2-Al_2O_3 composite.

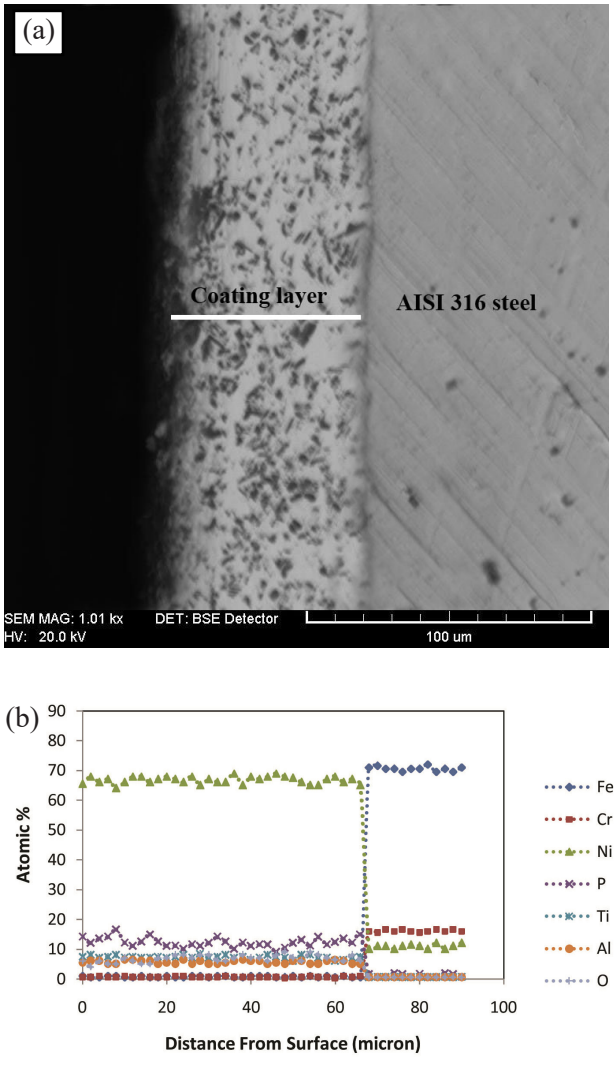

Fig. 4. Cross-section SEM image (a) and EDX analysis (b) of the sample coated with Ni-P-TiO_2-Al_2O_3 composite.

3.2. Isothermal Oxidation Behavior

A comparison between the weight gain of the uncoated and Ni-P-TiO_2-Al_2O_3 composite coated samples versus oxidation time is shown in Fig 5. Weight gain for Ni-P-TiO_2-Al_2O_3 composite coated samples after 300 hours of oxidation was 0.58 mg/cm^2, while the uncoated sample after the same oxidation time was 1.63 mg/cm^2.

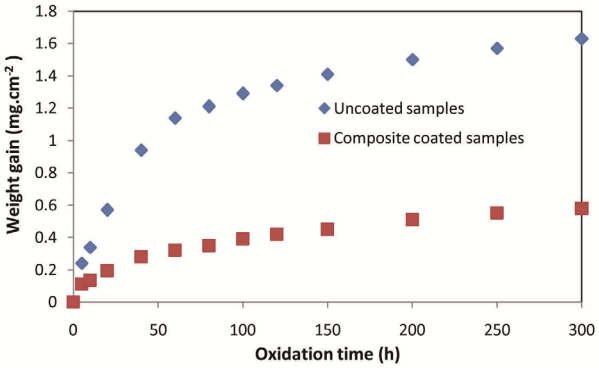

Fig. 5. Weight gain curves of uncoated and Ni-P-TiO_2-Al_2O_3 composite coated sample at 800 °C.

It can be observed that the mass gain of the Ni-P-Al_2O_3-TiO_2 composite coating was high in the early stage of oxidation (50 hr). However, thereafter, the rate of mass gain decreased rapidly, which indicated formation of a protective oxide scale. The mass gain of the uncoated alloy was higher than that of the Ni-P-Al_2O_3-TiO_2 composite coating after the first 50 hours of oxidation. However, the mass gain decreased considerably after 50-hr of oxidation because of the little oxide scale spalling and the good protection of the oxide scale. No spallation was observed for the Ni-P-Al_2O_3-TiO_2 composite coating after 300 hours of oxidation. These observations suggested that the Ni-P-Al_2O_3-TiO_2 composite coating possess much superior oxidation resistance compared to that of the uncoated steel.

As can be seen in Fig 5, the weight-gain kinetics of the uncoated substrate for 300 hours at 800 °C under isothermal oxidation consists of two stages. The first stage has a faster rate than the second one. When chromium-containing steel is exposed to an oxidizing atmosphere, chromium is oxidized and a Cr_2O_3-resistant scale is formed. As a result, the oxidation rate decreases over time due to the formation of the Cr_2O_3 scale [36-39].

The oxide layer grows faster up to 60 hours of isothermal oxidation comparing with the longer times. This is due to the nonappearance of a protective layer on the surface which rises the oxidation rate as a result of increasing the thickness of the oxide layer at the initial oxidation time. With the passage of time, the oxidation rate decreases because of the development of the Cr_2O_3

scale and reduces the growth rate of the oxide layer.

Comparison of the square of weight-gain of Ni-P-TiO_2-Al_2O_3 composite coating and uncoated substrate as a function of the oxidation time at 800 °C is shown in Fig 6.

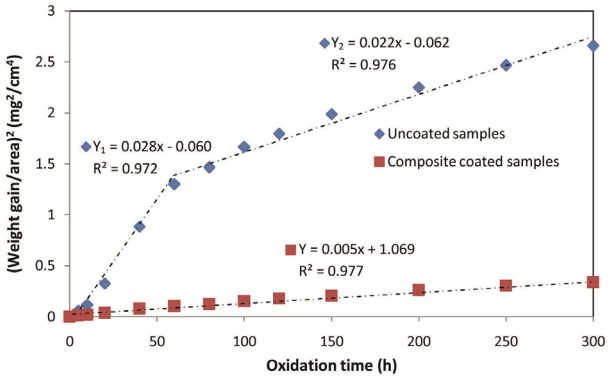

Fig. 6. Square weight gain of uncoated and coated samples with Ni-P-TiO_2-Al_2O_3 composite at 800 °C for 300 hours.

To calculate the oxidation rate, the weight gains obtained from the uncoated samples, and the coated ones were plotted in equation (1) to achieve a constant oxidation rate [40]:

$$\left(\frac{\Delta W}{A}\right)^2 = k_p t \qquad \text{Eq. (1)}$$

Δm is the weight increase in mg, A is the surface area in cm^2, k_p is parabolic rate constant and t is the oxidation time in s, and A is the surface area in cm^2. These constants are equal to the slope of the lines drawn in Fig. 6 The constant values of the oxidation rate related to the uncoated steel and Ni-P-Al_2O_3-TiO_2 composite coated steel at 800 °C are given in table 3.

The amount of kp obtained for the coated samples is 1.2×10^{-13} $g^2cm^{-4}s^{-1}$, which is lower than the one of the uncoated specimens in both stages in which it, indicates slower absorption of oxygen.

Fig. 7 shows the SEM image of uncoated steel (Fig. 7a) and composite coated steel (Fig. 7b) after 300 hours of isothermal oxidation at 800 ° C. As can be seen, there are some cracks on the surface of the uncoated sample (Fig. 7a). The cracks are on account of the development of defects in the oxide layer-interface, as well as the mismatch of the coefficient of thermal expansion of the oxide layer to the substrate [41]. The presence of the cracks causes oxygen to spread within the bed unhindered, resulting in faster oxidation. Also, chromium oxide is a P-type oxide that grows through the outward diffusion of chromium cations. Therefore, in long-term oxidation processes or oxidation at higher temperatures, vacant cations move inwards and accumulate in the oxide-metal interface, contributing to formation of po-rosity and cavity in this region, thereby reducing the adhesion of the scale to the substrate [42]. With the progression of oxidation, cracks are formed on the surface of the uncoated sample. The oxide layer also has a lower thermal expansion coefficient than the substrate. The difference in the coefficients of thermal expansion results in the formation of stresses; consequently, oxidation and oxide layer's growth over time will increase the amount of stress in the oxide layer [43].

As seen in Fig. 7b, there are no cracks in the composite coating. This shows the match of the thermal ex-pansion coefficient of the coating layer and the substrate. Figure 8 shows the X-ray diffraction pattern obtained from the uncoated sample (Fig. 8a) and the specimen coated with a Ni-P-TiO_2-Al_2O_3 (Fig. 8b) after 300 hours of oxidation at 800 °C. X-ray diffraction of the uncoated sample shows Cr_2O_3, Fe_2O_3, $MnCr_2O_4$, and $NiFe_2O_4$ phases. The formation of chromium oxide is due to the outward diffusion of chromium cation and the inward diffusion of oxygen anions. In the early stages, chromium is transmitted through ferrite grains with a small amount of volumetric diffusion [44, 45]. Simultaneously, manganese and iron ions (Mn^{2+} and Fe^{3+}) are diffusing through the chromium oxide layer reacting with oxygen and, chromium and, forming Mn-Cr spinel and iron oxide. The thickness of the chromium layer increases with increasing oxidation time; and ultimately, cracks in some surface areas [44]. The reason for the formation of Mn-Cr spinel on the chromium layer is the diffusion rate of the elements through the chromium layer. The diffusion rate

Table 3. Parabolic rate constant for uncoated and Ni-P-TiO_2-Al_2O_3 composite coated samples.

	Oxidation time (hr)	kp (g^2 cm^{-4} s^{-1})
Coated steel	0-300	1.2×10^{-13}
Uncoated steel	0-60	8.9×10^{-11}
	60-300	4.6×10^{-12}

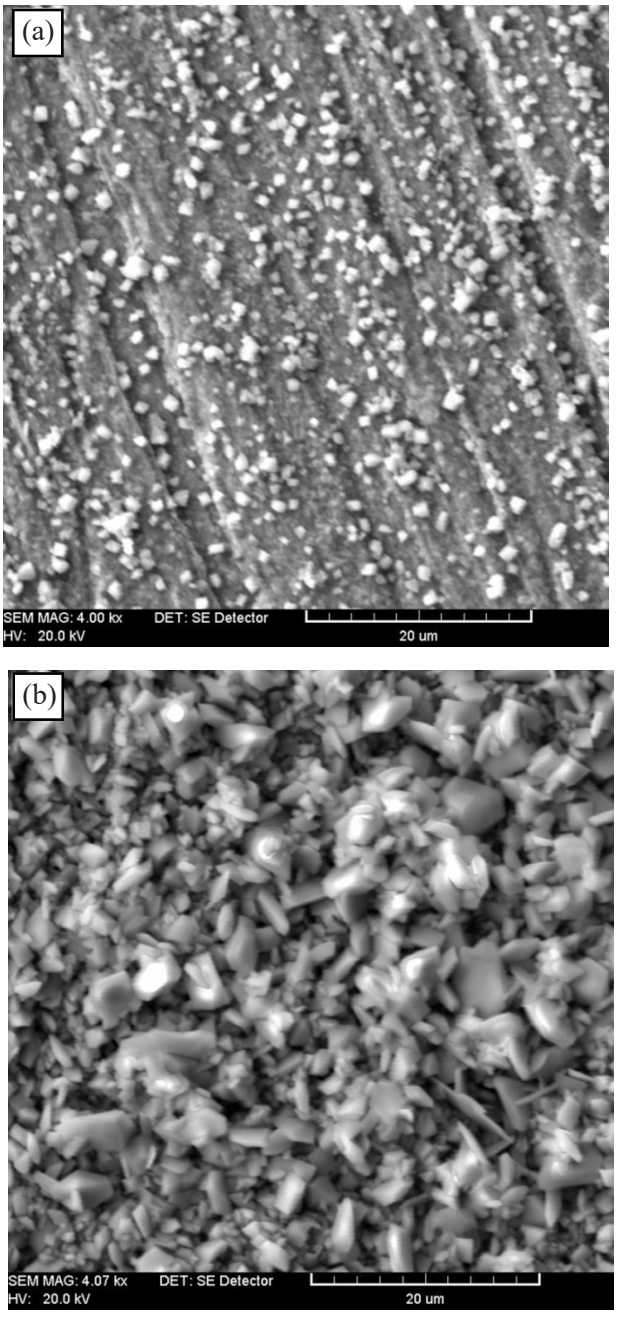

Fig. 7. SEM surface morphology of (a) uncoated and (b) coated specimen with Ni-P-TiO_2-Al_2O_3 com-posite after 300 hours of oxidation at 800 °C.

of Mn^{2+} in the chromium layer is greater than the other elements [45]. The diffusion coefficient of chromium, iron, and nickel ions is similar but less than the manganese diffusion coefficient. For this reason, manganese-rich spinel is one of the main oxide phases, even in steels with less than 1% manga-nese [46, 47]. Pyramidal particles found on the surface of the uncoated steel are $(Mn, Cr)_3O_4$ spinels (Fig. 7a); which is confirmed by XRD analysis (Fig. 8a). Increasing the weight gain of the uncoated samples indicates that chromium has failed to protect the substrate against oxidation.

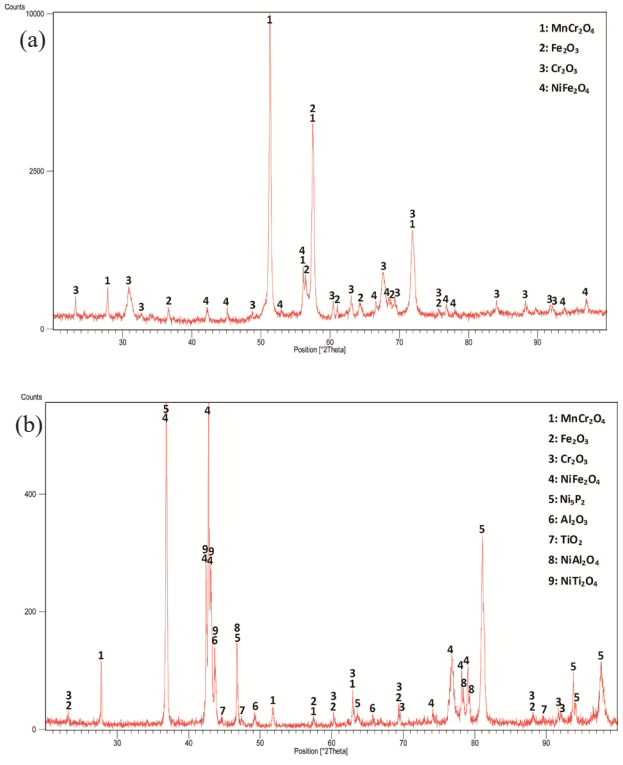

Fig. 8. XRD analysis of the sample (a) without coating and (b) coated with Ni-P-TiO_2-Al_2O_3 compo-site after 300 hours of oxidation at 800 °C.

The phases formed on the surface of the coated steel consist of $NiFe_2O_4$, Ni_5P_2, Al_2O_3, TiO_2, $NiAl_2O_4$, $NiTi_2O_4$, $MnCr_2O_4$, Fe_2O_3, and Cr_2O_3. The presence of $NiFe_2O_4$ and Fe_2O_3 phases have been confirmed by other researchers [48-50].

Over time owing to the formation of $NiFe_2O_4$,$NiAl_2O_4$, and $NiTi_2O_4$ phases, the diffusion of cations such as Ni, Cr will decrease and as a result, the oxidation resistance of the coating will increase after the first stage [28, 29]. Also, it can be stated that after the formation of $NiFe_2O_4$, $NiAl_2O_4$, and $NiTi_2O_4$ phases, the oxidation mechanism changes. In the first step, the mechanism includes the outward move-ment of chromium ions; however, with the formation of $NiFe_2O_4$, $NiAl_2O_4$, and $NiTi_2O_4$ phases, the outward movement of the chromium ions decreases. As a result, the moving mechanism of chromium cations shifts to the movement of oxygen anions. Therefore, due to the much lower diffusion coefficient of oxygen than that of chromium cations, oxidation resistance improves [51]. Also, the existence of Al_2O_3 and TiO_2 as the second phase in the coating matrix reduces the bulk diffusion of chromium and leads to an improvement in the oxidation resistance. Another theory illustrating better resistance of the Ni-P-TiO_2-Al_2O_3 composite coatings is that oxide particles of TiO_2 and Al_2O_3 are stable at 800°C. These particles increase high temperature oxidation

resistance. They prevent the outward movement of cations at high temperatures and reduce the oxidation rate [52-54]. Oxidation is initially performed through interactions between oxygen and nickel particles on the composite surface and then is controlled by diffusion. At the beginning of the diffusional oxidation, the amount of $NiAl_2O_4$ is low and the nickel ions diffusion is controlled by the boundaries of Al_2O_3 and TiO_2 [55]. Ni particles react with Al_2O_3 particles according to equilibrium equation2.

$$2Ni + 2Al_2O_3 + O_2 = 2NiAl_2O_4 \quad [28] \qquad \text{Eq.(2)}$$

At this stage, a dense $NiAl_2O_4$ layer forms on the surface, and then, oxidation is controlled by oxygen diffusion between aluminum oxide and $NiAl_2O_4$ spinel. The oxidation product, $NiAl_2O_4$, is dense and protective [56]. The corresponding standard free energy of formation of $NiAl_2O_4$ is based on equation 3.

$$\Delta G^o = -1499-2.31T(\pm 150)\ cal.mol^{-1}.\ [57] \qquad \text{Eq.(3)}$$

Based on equation 3 standard free energy of formation of $NiAl_2O_4$ at 800 ºC is about 3977 $cal.mol^{-1}$. Al_2O_3 particles increase oxidation resistance because the embedded Al_2O_3 particles provide an elemental-reactive effect on the growth of NiO particles in composite coatings. During oxidation, the separation of Al-ions occurs at the boundary of NiO grains; and, Al_2O_3 particles connect between grains and prevent nucleation and crack propagation, by trapping the NiO grains [57]. Cracking and oxidation of the oxide layer in isothermal oxidation are associated with the distribution of thermal stresses in oxide scales. Dur-ing heating and cooling, the oxide scale is subjected to thermal stresses. Other parameters such as oxide growth rate, maximum and minimum temperatures, heating and cooling rate, oxidation time, and chemical composition of the alloy also affect the isothermal oxidation resistance [58]. Fig. 9 shows the cross-sectional SEM image (Fig. 9a) and the elemental distribution across the oxide scale of the uncoated sample (Fig. 9b) after 300 hours of isothermal oxidation at 800°C. The grown oxide scale on the surface of the uncoated steel consists of two layers. The thicknesses of the first and second layers are respectively about 10 and 25 µm, respectively (Fig. 9a).

Also, fig. 10, shows the SEM cross-sectional image (Fig. 10a) and the elemental distribution across the oxidized coating layer of Ni-P-TiO_2-Al_2O_3 coated sample (Fig. 10b) after 300 hours of oxidation at 800°C. The cross-sectional image of the coated specimens also shows two layers of oxidized coating and chromium oxide on the substrate (Fig. 10b). The outer layer shows the oxidized coating layer, and there is a chromium layer underneath this layer. The thickness of the chromium layer is about 8 µm. The Ni-P-TiO_2-Al_2O_3 composite coating reduces the growth of the chromium layer in comparison with the uncoated substrate. This is due to the limitation of

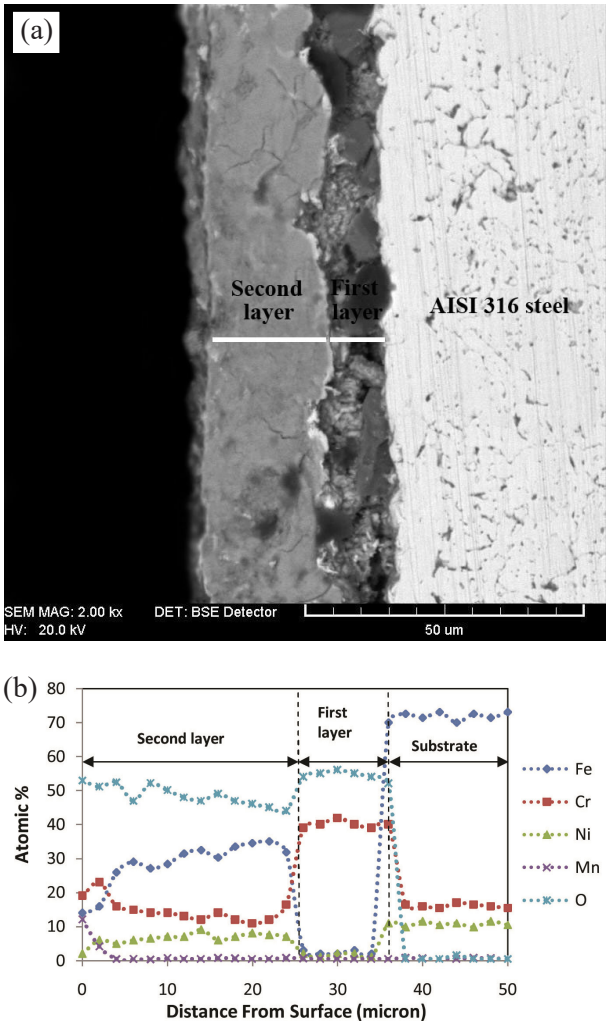

Fig. 9. Cross-sectional SEM image (a) and EDX analysis (b) of uncoated sample after 300 hours of iso-thermal oxidation at 800 ºC.

the penetration rate of chromium cations by the coating layer [59,60]. The decrease in the chromium layer's growth in the coated specimens is consistent with the de-cline in the intensity of chromium peaks in these specimens compared with the uncoated substrate (Fig. 10b and Fig. 8b).

3.3. Cyclic Oxidation Behavior

Fig. 11 shows the weight gain curve of the coated and uncoated samples versus the number of cycles. In all cycles, coated samples show a lower weight gain than the uncoated ones. Weight gains for sam-ples with Ni-P-TiO_2-Al_2O_3 coating and the uncoated ones after 50 cycles were 0.24 mg/cm^2 and 1.42 mg/cm^2, respectively. The lower weight gain of samples coated with Ni-P-TiO_2-Al_2O_3 and the absence of cracks in the coating demonstrates higher resistance of the composite coatings against thermal stresses.

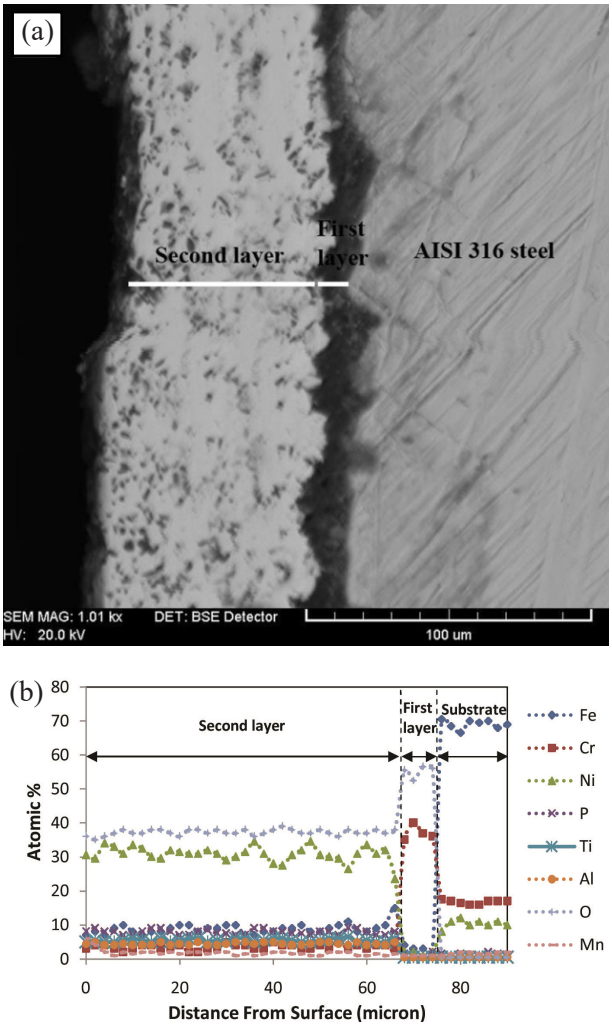

Fig. 10. Cross-sectional SEM image (a) and EDX analysis (b) the sample coated with Ni-P-TiO_2-Al_2O_3 composite after 300 hours of isothermal oxidation at 800 ºC.

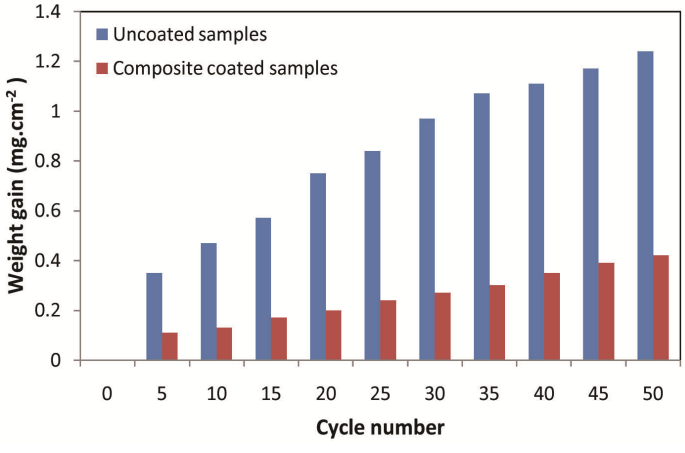

Fig. 11. Weight gain curves of uncoated and coated Ni-P-TiO_2-Al_2O_3 sample during cyclic oxidation.

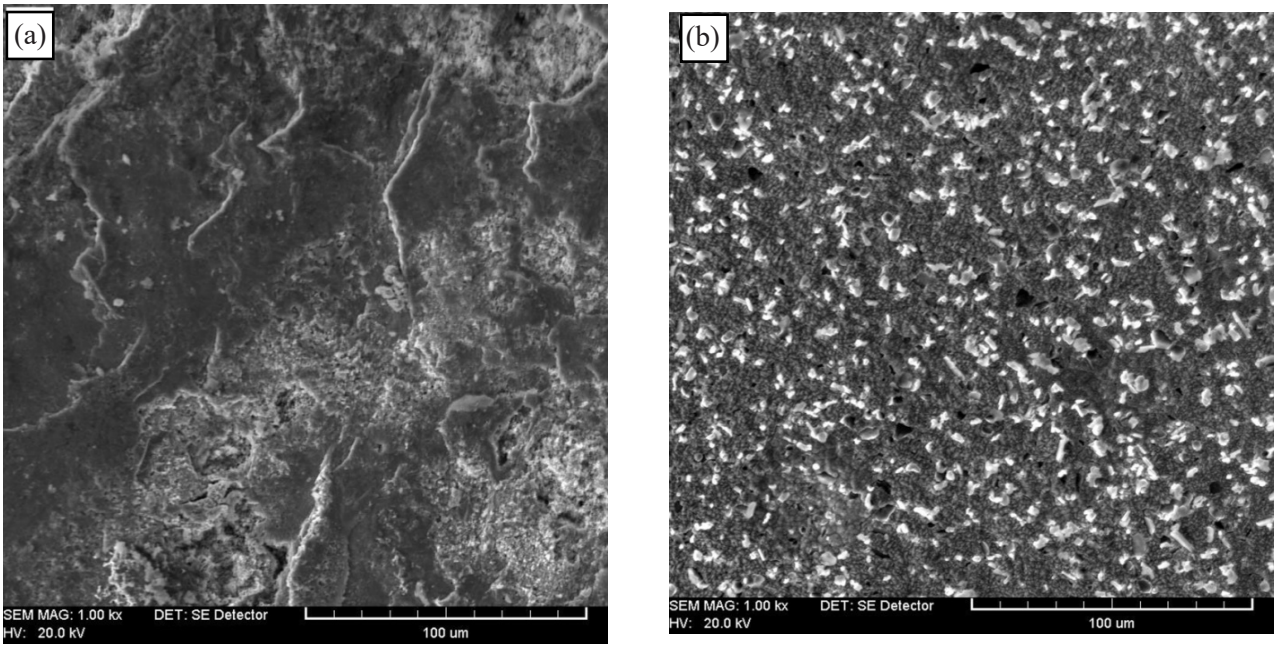

Fig. 12. SEM surface morphology of (a) uncoated and (b) coated specimens with Ni-P-TiO_2-Al_2O_3 composite after 50 cycles of oxidation at 800 °C.

The SEM image of coated and uncoated samples after 50 cycles of oxidation is shown in Fig. 12. As shown, there are many cracks on the surface of uncoated samples after 50 cycles of oxidation (Fig. 12a). Crusting and cracking are due to the mismatching of the coefficient of thermal expansion in the oxide layer and the substrate [61-65]. The discrepancy between the thermal expansion coefficient of chromium and spinel (Mn, Cr)$_3O_4$ with the substrate and the low resistance of (Mn, Cr)$_3O_4$ spinel against thermal stresses resulted in cracking and scaling of the oxide layer which has also been observed by other researchers [20,21]. Cracked crust provides outward and inward diffusion pathways for cations and ani-ons, and through the easy migration of ions; the oxide layer grows at a higher rate [36-40]. As can be ob-served, there is no crack on the surface of the coated specimen (Fig. 12b). The changing process of weight, based on the oxidation time was similar for both samples subjected to cyclic oxidation and isothermal oxidation. The only difference is in the weight gain increase of the samples in this case.

The number of thermal stresses in cyclic oxidation is more in comparison with isothermal oxidation. Thermal stresses lead to cracking and these cracks are easy diffusional paths for inward diffusion of oxygen anion and outward diffusion of metallic cations. Therefore, the fast growth of oxide layer causes higher weight gain, which has been already observed in our previous research [52-56]. On the surface of the uncoated steel, there are signs of scaling of the oxide scale in some areas. The reason for the defects on the surface of the uncoated specimen is the thermal expansion coefficient mismatch of the oxide scale and the substrate [41]. On the coated samples, there is no sign of cavity or cracks after the isothermal ox-idation test. The reason for this is the thermal expansion coefficient match of the oxide layers with that the metallic substrate [39, 40]. In all parts of the coated samples, the coating surface is almost dense and consists of spinel oxide particles. It seems that only micro-cavities are observed among spinel particles. These cavities are more likely to appear in composite coatings owing to the greater difference in the coefficient of thermal expansion of the reinforcing particles (Al_2O_3 and TiO_2) compared to the coating layer and the substrate. This leads to the formation of micro-cracks during thermal cycles.

Conclusions

- Composite coating of Ni-P-TiO_2-Al_2O_3 was formed on AISI 316 steel through electroplating. The fabricated layer was dense without pores and cracks. Isothermal and cyclic oxidation tests were applied to uncoated and coated samples.
- Weight gain during oxidation tests for samples coated with a Ni-P-TiO_2-Al_2O_3 was lower compared with the uncoated substrate. This was due to the oxidation resistance of the coating layer in comparison to the uncoated substrate.
- The formation of $NiFe_2O_4$, $NiAl_2O_4$, and $NiTi_2O_4$ phases and the existence of Ni_5P_2, TiO_2, and Al_2O_3 oxides in the coated samples led to reduction of the oxide layer's growth and the decrease of the weight

gain of the coated samples. The reason for this was the limitation of outward diffu-sion of chromium cation and inward diffusion of oxygen anion.

- The formed oxide film of the composite coating was made up of two layers, the outer layer was rich in nickel and had a small amount of iron and the inner layer was rich in chromium. The formed outer layer prevented the outward diffusion of chromium. Therefore, the thickness of the chromium-rich oxide layer related to the coated specimens in the isothermal oxidation was significantly reduced compared to the uncoated alloy.
- In cyclic oxidation, coated samples showed significantly better resistance to thermal stresses and cracks in comparison with uncoated samples. This is due to better oxidation resistance of Ni-P-TiO_2-Al_2O_3 composite coating comparing with the uncoated substrate.

References

[1] Z. Yang, G. Xia, S. P. Simner and J. W. Stevenson: J. Electrochem. Soc., 152(2005), 1896.
[2] R. Trebbels, T. Markus and L. Singheiser: J. Electrochem. Soc., 157(2010), 490.
[3] C. Hsu: Surf. Coat. Technol., 231(2013), 380.
[4] I. Haq, U. Akhtar, T. Khan and A. Ali Shah: Surf. Coat. Technol., 235(2013), 691.
[5] B. Szczygiel and M. Kolodziej: Electrochim. Acta., 50(2005), 4188.
[6] S. L.Kuo: Mater. Chem. Phys., 86(2004), 5.
[7] H. Sheu, P. Huang, L. Tsai and K. Hou: Surf. Coat. Technol., 235(2013), 529.
[8] T. Tamilarasan, R. Rajendran, G. Rajagopaland J. Sudagar: Surf. Coat. Technol., 276(2015), 320.
[9] M. Chou, M. Ger, S. Ke, Y. Huang and S. Wn: Mater. Chem. Phys., 92(2005), 146.
[10] B. G. Mellor: Surface coating for protection against wear, CRC Press, Boca Raton, Florida, (2006).
[11] P. Sahooand, S. K. Pal: Tribol. Lett., 289(2007), 191.
[12] Sh. Guangjie, Ch. Ling, W. Fengyan, Ch. Junming and Q. Xiujuan: Mater. Chem. Phys., 90(2005), 327.
[13] A. Mosavi, and H. Ebrahimifar: Int. J. Hydrogen Energy., 45(2020), 3145.
[14] H. Gül,F. Kılıc, S. Aslan,A. Alp and H. Akbulut: Wear., 267(2009), 976.
[15] L. Chen, L. Wang, Z. Zeng and J Zhang: Mater. Sci. Eng., A, 434(2006), 319.
[16] W. Shao, D. Nabb, N. Renevier, I. Sherrington and J. K. Luo: Mater. Sci. Eng., 40(2012), 1.
[17] X. J. Sunand, J. G. Li: Inst.Mater. Sci. Eng., 28(2007), 223.
[18] J. M. Huang, Y. Li,G. F.Zhang, X. D. Hou and D. W. Deng: Surf. Eng., 29(2013), 194.
[19] S. Geng, S. Qi, Q. Zhao, S. Zhu and F. wang: Int. J. Hydrogen Energy, 37(2012), 10850.
[20] N. Shaigan, W. Qu , D. J. Ivey and W. Chen: J. Power Sources, 195(2010), 1529.
[21] E. Rudnik, L. Burzyńska, L. Dolasiński and M. Misiak: Appl. Surf. Sci., 256(2010), 7414.
[22] L. Burzyńska, E. Rudnik, J. Koza, L. Blaz and W. Szymanski: Surf. Coat. Technol., 202(2008), 2545.
[23] W. Chen., Y. He and W. Gao: Surf. Coat. Technol., 204(2010), 2487.
[24] C.S. Lin, C.Y. Lee, C.F. Chang and C.H. Chang: Surf. Coat. Technol., 200(2006), 3690.
[25] D. Thiemig and A. Bund: Surf. Coat. Technol., 202(2008), 2976.
[26] T. Lampke, A. Leopold, D. Dietrich, G. Alisch and B. Wielage: Surf. Coat. Technol., 201(2006), 3510.
[27]M. Abaei, M. Zandrahimi and H. Ebrahimifar: Int. J. Mater. Res., 110(2019), 253.
[28] E. Khoran, M. Zandrahimi and H. Ebrahimifar: Oxid. Met., 91(2019), 177.
[29] X. Peng, D. Ping, T. Li and W. Wu: J. Electrochem. Soc.,145(1998), 389.
[30] X. Peng, T.Li and W. Wu: Oxid. Met., 51(1999), 291.
[31] W. Zhou, Y.G. Zhao, W. Li, B. Tian, S. W. Hu and Q.D. Qin: Mater. Sci. Eng., A, 458(2007), 34.
[32] Y. J. Xue, H. B.Liu, M. M. Lan, J. S. Li and H. Li: Surf. Coat. Technol., 204(2010), 3539.
[33] N. S. Qu, D. Zhu and K. Chan: Scr. Mater., 54(2006), 1421.
[34] A. Holt and P. Kofstad: Solid State Ionics, 69(1994), 137.
[35] A.S. Khanna: Introduction to high temperature oxidation and corrosion, ASM International, Materials Park, OH, (2002), 128.
[36] M. Stanislowski, E.Wessel, K. Hilpert, T. Markus and L. Singheiser: J. Electrochem. Soc., 154(2007), 295.
[37] G. C. Wood and D.P. Whittle: J. Electrochem. Soc., 115(1968), 126.
[38] S. Fontana, R. Amendola, S. Chevalier, P. Piccardo, G. Caboche, M. Viviani, R. Molins and M. Sen-nour: J. Power Sources, 171(2007), 652.
[39] F. Saeidpour, M. Zandrahimi and H. Ebrahimifar: Corros. Sci., 153(2019), 200.
[40] A. Petric and H. Ling: J. Am. Ceram. Soc., 90(2007), 1515.
[41] W. Qu, L. Jian, G. Douglas Ivey and J. M. Hill: J. Power Sources., 157(2006), 335.
[42] R. E. Lobnig, H. P. Schmidt, K. Hennesen and H. J. Grabke: Oxid. Met., 37(1992), 81.
[43] M.G. C. Cox, B. Mcenaney and V.D. Scott: Philos. Mag., 26(1972), 839.
[44] H. Kurokawa, K. Kawamura and T. Maruyama: Solid State Ionics, 168(2004), 13.
[45] S. K. Mitra, S.K.Roy and S. K. Bose: Oxid. Met., 34(1990), 101.
[46] S. K. Mitra, S.K.Roy and S. K. Bose: Oxid. Met., 39(1993), 221.
[47] I. M. Allam, D.P.Whittle and J. Stringer: Oxid. Met.,

12(1978), 35.
[48] L. Zhu, X.Peng, J. Yan and F. Wang: Oxid. Met., 62(2009), 411.
[49] T. C. Wang, R. Z. Chen and W. H. Tuan: J. Eur. Ceram. Soc., 23(2003), 927.
[50] H. V. Pham, D. Maruoka and M. Nanko: J. Asian Ceram. Soc., 4(2016), 120.
[51] K. H. Hou and Y. C. Chen: Appl. Surf. Sci., 257(2011), 6340.
[52] H. Ebrahimifar and M. Zandrahimi: Surf. Coat. Technol., 206(2011), 75.
[53] H. Ebrahimifar and M. Zandrahimi: Oxid. Met., 84(2015), 329.
[54] H. Ebrahimifar and M. Zandrahimi: Oxid. Met., 84(2015), 129.
[55] H. Ebrahimifar and M. Zandrahimi: Ionics, 18(2012), 615.
[56] H. Ebrahimifar and M. Zandrahimi: Solid State Ionics, 183(2011), 71.
[57] K.T.Jacob and C.B.Alcock: J. Solid State Chem. 20(1977), 79.
[58] E. N'Dah, S. Tsipas, M. P. Hierro and F. J. Pe´rez: Corros. Sci., 49(2007), 3850.
[59] S. Molin, B. Kusz, M. Gazda and P. Jasinski: J. Power Sources, 181(2008), 31.
[60] F. Saeidpour, M. Zandrahimi and H. Ebrahimifar: Int. J. Hydrogen Energy, 44(2019), 3157.
[61] W.Z. Zhu and S.C. Deevi: Mater. Res. Bull., 38(2003), 957.
[62] L. Cooper, S. Benhaddad, A. Wood and D. G. Ivey: J. Power Sources, 184(2008), 220.
[63] T. Horita, Y. Xiong, K. Yamaji, N. Sakai and H. Yokokawa: J. Electrochem. Soc., 150(2003), 243.
[64] H. Ebrahimifar and M. Zandrahimi: Oxid. Met., 75(2010), 125.
[65] M. Landkof, A.V. Levy, D.H. Boone, R. Gray and E. Yaniv: Corros. Sci., 41(1985), 344.